# Absolute efficiency and time-response measurement of single-photon detectors

P. G. Kwiat, A. M. Steinberg, R. Y. Chiao, P. H. Eberhard, and M. D. Petroff

Using correlated photons from spontaneous parametric downconversion, we have measured both the absolute quantum efficiencies and the time responses of four single-photon detectors. Efficiencies as high as (76.4 ± 2.3)% (at 702 nm) were seen, which to our knowledge are the highest reported single-photon detection efficiencies. An auxiliary retroreflection mirror was found to increase the net detection efficiency by as much as a factor of 1.19. The narrowest time profile for coincidences between two detectors displays a peak with 300 ps FWHM. We also investigated the presence of afterpulses and the effects of saturation and varying device parameters.

*Key words:* Quantum efficiency, photon counting, avalanche photodiode.

## 1. Introduction

By means of the process of spontaneous parametric downconversion in a crystal with a nonlinear susceptibility, it is possible to create pairs of photons that are highly correlated in time and reasonably well collimated. Such a two-photon source is ideal for making measurements of the absolute detection efficiency and temporal response of single-photon counting detectors, such as photomultipliers and avalanche photodiodes. Here we describe a series of such measurements made on a pair of solid-state photomultipliers (SSPM's) from Rockwell[1] and on a pair of single-photon counting modules (SPCM's, in this case SPCM-200-PQ's) from EG&G.[2] The highest efficiencies measured were (70.9 ± 1.9)% at 633 nm and (76.4 ± 2.3)% at 702 nm with a SSPM and a SPCM, respectively. However, subsequent tests on the SSPM's revealed possible degradation of transmission in the input fibers, and there were substantial reflection losses within the SPCM's. At present it is difficult to determine adequate correction factors accurately for these effects. Nevertheless, to our knowledge our results are the highest reported single-photon detection efficiencies; they are important for quantum cryptography and loophole-free tests of Bell's inequalities, as well as for more prosaic applications such as photon correlation spectroscopy and velocimetry.[3] Note that, although other photodetectors (e.g., silicon or InGaAS P-I-N photodiodes) can be fast and display very high sensitivities (one recent article[4] measured a quantum efficiency of 94%), these cannot detect single photons.

Section 2 briefly describes the source of correlated photons in our experiments, whereas Section 3 discusses the use of such a source to measure absolute quantum efficiencies. Descriptions of the detectors, detailed experimental setup, and typical procedure are given in Sections 4, 5, and 6, respectively. In Section 7 our efficiency results are presented; we also attempt to list the various sources of systematic error, corrections to apply to the data, and the final corrected efficiencies. In Section 8 the results of several related measurements are described, including the time-response characteristics of the detectors, the effects of saturation, and the presence of afterpulsing in the SPCM's. Our conclusions are presented in Section 9. A discussion of statistical error analysis appropriate for our results is presented in Appendix A.

## 2. Source

The process of spontaneous parametric downconversion has been well studied.[5,6] In a crystal with a nonlinear $\chi^{(2)}$ susceptibility, a pump photon at frequency $\omega_p$ may split into two correlated photons at

M. D. Petroff is with the Rockwell International Corporation Science Center, 3370 Miraloma Avenue, Anaheim, California 92803. When this research was performed, the other authors were with the University of California, Berkeley, Berkeley, California 94720; P. G. Kwiat, A. M. Steinberg, and R. Y. Chiao are with the Department of Physics and P. H. Eberhard is with the Lawrence Berkeley Laboratory. P. G. Kwiat is now with the Institut für Experimentalphysik, Universität Innsbruck, Technikerstrasse 25, 6020 Innsbruck, Austria.

Received 12 April 1993.
0003-6935/94/101844-10$06.00/0.

frequencies $\omega_1$ and $\omega_2$. The process must satisfy energy conservation, $\omega_p = \omega_1 + \omega_2$, and momentum conservation, $\mathbf{k}_p = \mathbf{k}_1 + \mathbf{k}_2$, inside the crystal. This last relation leads to the well-known phase-matching conditions. The net result is that the downconverted photons typically exit the crystal at small angles with respect to the pump beam (less than 3° in our case), with photons of the same pair propagating in a plane containing the pump wave vector $\mathbf{k}_p$. Because various geometries satisfy the phase-matching constraints, a broad spectrum of downconverted light is possible; each color emerges from the crystal in a cone (about the pump-beam axis) whose opening angle depends on wavelength (and on the angle between the pump beam and the crystal optic axis, 50.7°). The angles for the colors employed in our tests are listed in Table 1. In practice, one selects these colors by using irises and filters before a detector.

## 3. Method

Because photons produced in spontaneous downconversion are *always* produced in *pairs,* with strong time correlation, they are ideal for absolute calibrations of photon detectors. The detection of one of the photons guarantees with certainty the presence of a photon at the conjugate detector. The technique, first proposed by Klyshko,[7] and used by Rarity *et al.*[8] to determine the efficiency of an RCA (now EG&G) silicon avalanche photodiode, is simple: Direct one photon of each pair to a trigger detector, and arrange the optics in order to catch all the conjugate photons with the detector whose efficiency is to be determined. For some time interval $T$ both the number of singles at the trigger detector and the number of coincidence counts between the detectors are measured. If the total number of emitted pairs is $N$, then the number of singles seen at the trigger detector is $N_t = \eta_t N$, whereas the number of coincidences is $N_{ct} = \eta_c \eta_t N$, where $\eta_t(\eta_c)$ is the detection efficiency at the trigger (conjugate) detector.[9] Assuming no external losses on the path to the conjugate detector, one can determine the efficiency $\eta_c$ simply by taking the ratio $N_{ct}/N_t$.

In practice, the simple formula mentioned above has to be modified to account for the presence of unwanted counts and the loss of desired counts. First, in addition to the desirable correlated photons, each detector will also possess a number BG of background counts, consisting of unwanted external light, dark counts within the detector, and possibly electronic noise. The true number of singles $N_t$ is then the measured quantity $S_t$ minus the background $\mathrm{BG}_t$ (determined in a separate measurement with the downconverted beams blocked for a duration $T_{\mathrm{BG}}$), weighted by the ratio of the two measurement times, $r_{\mathrm{BG}} \equiv T/T_{\mathrm{BG}}$. Similarly, $N_c = S_c - \mathrm{BG}_c r_{\mathrm{BG}}$, where the subscripts refer to counts at the conjugate detector. Second, there will be spurious coincidence counts caused by the finite duration $w$ of the coincidence window. The true number of coincidences $N_{ct}$ is then the measured value $C$ minus the accidental counts, $A \approx [S_c S_t - \eta_c S_c (S_t - \mathrm{BG}_t r_{\mathrm{BG}})]w/T$ (see Appendix A). In practice, one uses as small a coincidence window as possible (of the order of tens of nanoseconds) while still catching all the true coincidence counts. Note that some photodetectors are known to possess trapping states, so some fraction of the incident photons produce extra electronic signals at some undetermined time (which can be as large as seconds) after the typical time for such a signal.[10] The presence of such afterpulses in the trigger rate reduces the measured conjugate efficiency, because they appear as real trigger photons without conjugate partners. For our trigger detector (a SPCM) fewer than 0.01% of the counts were echoed in this fashion, so the effect on the efficiency measurements was negligible (see Section 8).

The last major correction factor stems from the loss of photons before they reach the detector, as a result of unwanted reflections, scattering, or absorption. For example, any uncoated glass–air interface will yield a loss of approximately 4%. This interface may be antireflection coated to reduce the loss significantly. The detector surfaces themselves, if uncoated, would also cause sizable losses from Fresnel reflections. Thus the net detection efficiency $\eta_{t(c)}$ for each photon may be written as the product of the detector's efficiency $\eta_{t(c)}{}^d$ and the path transmissivity $\eta_{t(c)}{}^p$.

Combining of these effects, we can now calculate the conjugate detector efficiency in terms of other, measurable, quantities:

$$\eta_c{}^d = \frac{1}{\eta_c{}^p} \frac{C - A}{S_t - r_{\mathrm{BG}} \mathrm{BG}_t}. \tag{1}$$

Notice that the efficiency associated with the trigger photon, $\eta_t{}^d \eta_t{}^p$, does not appear in Eq. (1). Therefore, one strives to reduce $\mathrm{BG}_t$ as much as possible (by using narrow-band interference filters and small irises before the trigger detector), even though this may reduce the transmissivity $\eta_t{}^p$.

**Table 1. Cone Divergence Angles and Conjugate Wavelengths for Downconverted Light (Pump Wavelength, 351.1 nm)**

| Wavelength | | Half-Opening Angle (deg) for Wavelengths in Column 1 |
|---|---|---|
| Downconverted Light (nm) | Conjugate Photon (nm) | |
| 633 | 788 | 2.25 |
| 702 | 702 | 2.4 |
| 788 | 633 | 3.0 |

## 4. Detectors

We performed measurements on four single-photon detectors: two custom-modified SPCM's from EG&G Canada, Ltd. (SPCM-200-PQ's) and two SSPM's from Rockwell International Corporation. The SPCM's use thermoelectrically cooled silicon avalanche photodiodes (APD's) in the Geiger mode with passive quenching. These photodiodes have a small active area, $\sim(100\ \mu\mathrm{m})^2$; along with an improved gettering

method in their production, this leads to a typical dark-count rate of only 60 $s^{-1}$. Our model was customized for 30-V biasing over the breakdown voltage of 400 V to provide a faster time response amd higher efficiency. A detection event gives rise to a 50-ns, 2-V pulse, followed by a dead time measured to be 0.5 μs. The SPCM's possess an effective $k$ (the ratio of hole-to-electron ionization coefficients, averaged over the device structure) of only 0.002, to be contrasted with the $k$ = 0.02 for typical photon-counting APD's (e.g., RCA 30902 silicon APD). It has been shown theoretically that the probability for a single photoelectron to cause an avalanche depends on the value of $k$, with lower $k$'s leading to higher gains, other things (e.g., excess voltage, depletion layer width) being equal.[2,11] For our SPCM's, it is estimated that the ratio of δ (the field-dependent electron-ionization coefficient, integrated over the depletion width) at the operating voltage to δ at the breakdown voltage is greater than 1.1, so detector efficiencies in excess of 80% are not unexpected.[12]

The SSPM's are silicon devices based on impurity-band-to-conduction-band impact-ionization avalanches. These avalanches contain approximately $5 \times 10^4$ electrons localized within areas several micrometers in size. Because impurity bands are involved, much lower field strengths are required for impact ionization than in standard APD's, which use valence-to-conduction-band impact ionization; the typical SSPM bias is only 7 V. In addition, because they do not operate above the avalanche breakdown voltage, these devices are capable of distinguishing between single-photon detections, double-photon detections, etc. (i.e., two simultaneously detected photons will produce an output signal approximately twice as large as a single photon). SSPM's have previously been demonstrated (by using a relative efficiency measurement) to possess greater than 50% detection efficiency in the visible-light region and greater than 30% at 20 μm, and they are predicted to have possible efficiencies greater than 90%.[1] The dark counts were typically 7000 $s^{-1}$ for these detectors, which have an active area of ~(1 mm)$^2$. (Note that the dark-count rate per unit area is comparable with that of the SPCM.) For optimum performance the SSPM's require cooling to 6 K.

## 5. Experimental Setup

A schematic of one of the experimental setups used is shown in Fig. 1, with each component numbered; below we discuss each in turn. Losses associated with these components will be discussed in Section 7. A slightly simpler setup with no mirrors was used for some of the measurements with the SPCM's.

1. An argon-ion laser produced the vertically polarized 351.1-nm pump beam, with a full-angle beam divergence of 0.3 mrad and a beam diameter at the crystal of 2 mm. A black glass filter and an iris (2.2 mm) were used to remove unwanted laser fluorescence. Fixed and variable neutral-density filters were

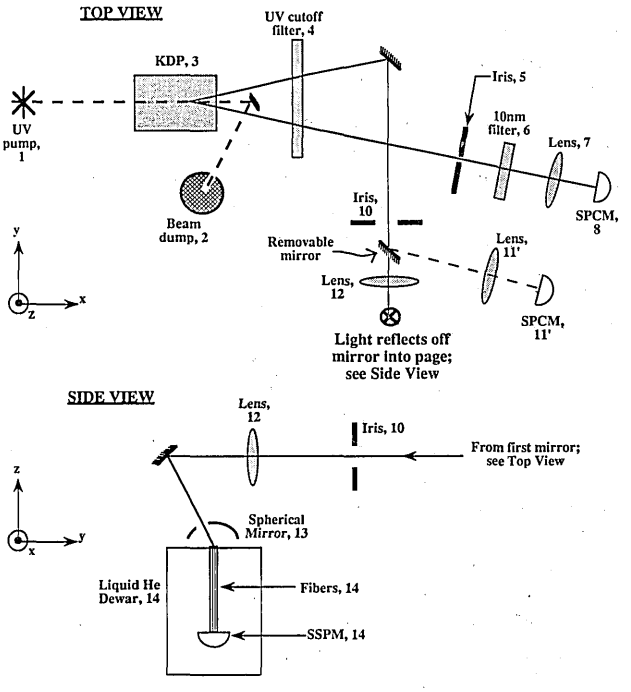


Fig. 1. Schematic of a typical experimental setup (see text for details).

used to control the input power. The net attenuation was typically optical density 4, so that the input to the crystal was typically 10 μW.

2. After passing through the crystal, the remaining, unscattered UV beam was directed by a small mirror to a beam dump.

3. A 10-cm long KDP crystal, cut for type-I phase matching, was oriented with its optic axis at 50.7° with respect to the pump beam. We measured the efficiencies by using two sets of conjugate photons. In the first set, both wavelengths were 702 nm. In the second set, the first wavelength was 633 nm and the second was 788 nm (the second wavelength is the color directed to the trigger detector). The crystal itself was housed in a sealed aluminum container, with index-matching fluid and fused-silica end windows. The crystal input face was antireflection (AR) coated for the UV; the output face was broadband AR (BBAR) coated to reduce output losses over the range 400–750 nm. Note that in some of the runs these directions were accidentally reversed, leading to an extra correction factor (see Section 7).

4. An UV cutoff filter was used to remove any scattered UV and laser fluorescence from both down-converted beam lines. This filter was BBAR coated to have high external transmittance (>99%) in the range 600–800 nm.

We now trace the components on the path to the trigger detector, a SPCM.

5. A small (1.4-mm) iris 1.5 m from the crystal was used to select the trigger photons. Because of phase-matching constraints in the downconversion

process, this iris determines the direction of the conjugate photons.

6. A 10-nm FWHM interference filter (at 702 or 788 nm) was used to select the trigger photons further and to remove most of the remaining background light. Because of energy conservation at the KDP source, this filter effectively determines the color (and hence the opening angle) of the conjugate photons.

7. A BBAR-coated 35-mm focal-length achromatic lens was used to focus the light onto the small active area, $\sim(100\ \mu m)^2$, of the trigger detector. In practice, the spot size was $\sim 70\ \mu m$.

8. The trigger detector, an EG&G SPCM-200-PQ, was aligned transversely and longitudinally (by micrometers) to maximize the singles count rate. The silicon diode surface was AR coated with a quarter-wave layer (at 630 nm) of SiO; the glass window of the housing was uncoated. The output of the SPCM was inverted, split, and directed to a counter (yielding the singles rate at the trigger detector), and to the START input of a time-to-amplitude converter (TAC).

9. To minimize the background we placed a black cardboard box (not shown in Fig. 1) over components 6–8, with a small opening to allow the trigger photons to enter. It was then found that the background rate was essentially indistinguishable from the intrinsic dark-count rate.

We now trace the components on the path to the conjugate detector, either a SSPM (unprimed numbers) or a second SPCM(11′), depending on the presence of a removable dielectric mirror.

10. A large iris (9.0-mm diameter) was used to accept all the photons conjugate to those passed by the 1.4-mm iris before the trigger detector. (Previous coincidence profile measurements had demonstrated that with this size iris fewer than 1% of the conjugate photons were lost.)

11′. The focusing lens, the second SPCM, and electronics in the conjugate path were identical to those in the trigger path (components 7 and 8), except that the signal was directed into the STOP of the TAC.

12. A 20-cm focal-length plano–convex lens (5.08 cm diameter, BBAR for low reflection in the range 600–1000 nm) was used to focus the light into an SSPM input fiber (see component 14 below). Another dielectric mirror was used to direct the conjugate photons downward to the SSPM fiber. The mirror was aligned so that the beam impinged on the fiber end at an angle of 15° from the normal as a way to facilitate the use of a spherical retroreflection mirror (see component 13).

13. For some of the measurements, a spherical dielectric mirror (35-mm radius of curvature, 5.08-cm diameter) was used to recapture photons that were reflected from either end of the fiber or from the surface of the SSPM itself. A small hole (0.635 cm) was made 15° off the symmetry axis to allow the beam to pass through. In practice the mirror was positioned with its center of curvature on the top of the fiber so that any light reflected off the fiber end was reflected back onto the fiber. Similarly, some of the light reflected off the detector itself traveled back up the fiber, filling the numerical aperture, and was refocused by the spherical mirror onto the fiber end. This led to substantial improvements in the efficiency (see Section 7).

14. We briefly examined four SSPM's, with greater detail on two of these. The efficiencies were similar for the four. Coupling light to the detectors was accomplished by using 19-cm-long acrylic fibers (750-μm core), which also served as cold filters to remove the excess of infrared background light. They have a rated attenuation of 0.43 dB/m at 633 nm and 0.62 dB/m at 702 nm. For the purpose of cooling the SSPM's to 6 K, a helium Dewar was suspended from an $X$–$Y$ translation stage, permitting coarse adjustments in the position of the relevant SSPM fiber and easy switching from one fiber to another (and hence from one detector to another).

The output of each detector was amplified first by a fast internal charge-sensitive preamplifier to 0.4 mV per photon, then twice more to make the signal appropriate for the following shaping circuitry. The typical pulse corresponding to a single-photon detection had an amplitude of 60 mV, a rise time of 10 ns, and a FWHM of 30 ns. The noise level was 35 mV.

After passing through an inverting transformer, the pulse was directed into a constant-fraction discriminator (CFD) with a 254-cm external shaping-delay cable. The discriminator threshold was set at −40 mV for most of the efficiency tests, as this was found to be sufficient for catching all the coincidence counts. A 50-ns blocking window was used to eliminate ringing. One of the CFD outputs was directed to a counter, yielding the singles rate at the SSPM. The other timing output was directed into the STOP input of the TAC.

The TAC output (for both types of conjugate detector) was then analyzed with a single-channel analyzer (SCA), affording better than a 100-ps time resolution. The SCA output was also directed to the counter, and data were saved to a PC.

Note that by simply switching the size of the irises (components 5 and 10) and moving the 10-nm filter (component 6) from one SPCM path to the other, we were able to exchange which SPCM acted as a trigger and which efficiency we were measuring. In this way the SPCM efficiency at 788 nm was also obtained (by using a 10-nm FWHM filter at 633 nm in front of component 11′).

### 6. General Procedure

The exact alignment procedure varied somewhat depending on a given run, but in general the trigger detector, trigger iris, conjugate detector, conjugate iris, and conjugate lens were adjusted to maximize the coincidence rate, and the ratio of this rate to the trigger-singles rate. This was done cyclically until no further improvements were obtained.

The input pump intensity was reduced until saturation effects were no longer a concern. In one test we confirmed that beam-line background (i.e., background counts from photons traveling along the main beam line to the trigger detector) was not an important concern by placing a second 10-nm FWHM filter at 702 nm before the trigger detector. (This was during the 702-nm efficiency test, so the detector already had one such filter before it.) The efficiency was unaltered to within statistical uncertainty.

The counts $S_c$, $S_t$, and $C$ were collected (in 1-s bins) for a time interval $T$, which was sufficient to permit adequate counting statistics; the background counts were collected for a similar interval. The accidental counts were calculated as stated in Section 3 (we confirmed this method in separate measurements of the coincidence rate, setting the electronic delay between the conjugate detector and the trigger detector to 100 ns). The collected data were analyzed for mean and uncertainty. Using Eq. (1), we then calculated the raw efficiency. The standard deviation was determined by using the following formula, which is derived in Appendix A:

$$\frac{\Delta\eta_c}{\eta_c} = \left[\frac{(1-\eta_c)C}{(C-A)^2} + \frac{2\mathrm{BG}_t}{(S_t - \mathrm{BG}_t)^2}\right]^{1/2}. \qquad (2)$$

### 7. Efficiency Results

For the SSPM tests, typical counting rates were $S_c \equiv S_{\mathrm{SSPM}} = 128{,}900\ \mathrm{s}^{-1}$, $S_t = 363 \pm 2\ \mathrm{s}^{-1}$, $\mathrm{BG}_t = 73.6 \pm 1.4\ \mathrm{s}^{-1}$, $C = 155 \pm 1\ \mathrm{s}^{-1}$, and $A = 0.6\ \mathrm{s}^{-1}$ (with a 20-ns gate window). Typical rates in the SPCM tests were roughly half of this, because of lower saturation rates and the fact that the SPCM had a much lower dark-count rate than the SSPM ($65\ \mathrm{s}^{-1}$ versus $7000\ \mathrm{s}^{-1}$). Note that the singles rates on the trigger and conjugate detectors are very different. This is due to the small iris and 10-nm filter in front of the former, and the large iris and no filter (other than the UV cutoff) before the conjugate detector.

We shall now attempt to list and account for the various systematic errors and their correction factors, which stemmed mainly from photon losses before the conjugate detectors. (Recall that losses of *trigger* photons do *not* influence the measured efficiency.) Using a photodiode and a He–Ne laser (operating at 633 nm) aligned to coincide with the conjugate beam of photons, we measured the transmissivity $\eta_c^p$ of the path leading to the conjugate detector. The light intensity just before the SSPM fiber (SPCM) was (91.3 ± 1.0)% [(93.9 ± 1.4)%] of that just after the crystal, because of losses in the cutoff filter, mirrors, and the focusing lens. One would expect ~1% loss at each interface, so the measured value is not unreasonable. A smaller correction factor was obtained with the simpler setup used in several of the measurements with the SPCM's.

Two sources of loss before the detector remain: reflection losses at the crystal, and scattering or absorptive losses within the crystal. We measured these, again using a He–Ne laser and a photodiode. The reflection intensity off the output face of the crystal container was (1.02 ± 0.12)%.[13] The internal transmission factor (i.e., subtracting out the reflection losses) for the entire length of the crystal was 0.954 ± 0.020. If one assumes that the downconverted photons are produced roughly at the center of the crystal, one finds an internal absorption–scattering loss of (2.3 ± 1.0)%. Combining this with the reflective losses, the total crystal correction factor is then 0.967 ± 0.010.

At 702 and 788 nm there was no convenient way to measure the predetector losses directly. For both cases, the actual paths of the light were similar to that of the 633-nm light (because the opening angles of the downconverted light cone are similar). Therefore the only difference is the wavelength dependence of reflection, absorption, and scattering losses. For simplicity, we assume the same path transmissivity $\eta^p(702\ \mathrm{nm}) = \eta^p(788\ \mathrm{nm}) = \eta^p(633\ \mathrm{nm})$. Note that this is probably a slight underestimate of the losses, as we expect the reflection losses to be greater for the longer wavelengths.

The effect of using a spherical mirror (component 13, Fig. 1) with the SSPM was tested. The mirror was inserted and aligned to give the highest efficiency; then it was removed and the singles and coincidence rates were remeasured. The mirror was found to increase the efficiency from (47.4 ± 0.6)% to (55.8 ± 0.7)% at 702 nm, and from (49.5 ± 0.5)% to (53.5 ± 0.4)% at 633 nm. A direct comparison of the results is difficult because varying the wavelength corresponded to realigning the system entirely. Clearly, however, the use of the mirror gave a significant improvement.

In a few of the tests on the SSPM, the timing window accepted only the main coincidence peak (described below), thereby excluding (11.9 ± 0.5)% of the coincidences. In addition, in examining the effects of SSPM bias (see Section 8), we found that the maximum efficiency was obtained at a slightly higher bias voltage than was typically used. When these various systematic errors are accounted for, the corrected efficiencies are as listed in Table 2, where we have included the results for two SSPM's and two SPCM's.

It is important to note that associated with each of the detectors there are other sources of loss that may

**Table 2. Corrected Single-Photon Absolute Detection Efficiencies of Two SSPM's and Two SPCM's**

| Wavelength (nm) | Corrected Efficiency (%) | | | |
|---|---|---|---|---|
| | SSPM 1[a] | SSPM 2[a] | SPCM 1 | SPCM 2 |
| 633 | 70.9 ± 1.9 | 69.5 ± 1.9 | 74.3 ± 2.0[b] | 65.0 ± 1.6 |
| 702 | | 66.3 ± 1.4 | 76.4 ± 2.3[b] | 75.4 ± 1.5[b] |
| 788 | | | 53.7 ± 1.4 | 54.4 ± 1.0 |

[a]The results listed include the improvements of a spherical retroreflection mirror on the efficiencies of the SSPM's.

[b]These results were obtained with a slightly simpler setup than that in Fig. 1, with no mirrors.

yet be reduced. Subsequent testing on the SSPM input fibers yielded a transmission of only (70 ± 5)%, including insertion losses. The expected loss caused by normal transmission and Fresnel losses is only 10%, which is consistent with the improvements observed with the spherical mirror. If any of the excess measured transmission loss were present during the efficiency experiment, the actual SSPM detector efficiencies will be somewhat higher. Adjusting for all the fiber losses would suggest device efficiencies as high as (93.7 ± 7.2)%. The SPCM detector is housed in a can with a glass window, which was not AR coated at all, implying 8% losses. The detector surface itself was BBAR coated, so that losses of 1% may be expected here. If these interfaces all had multilayer coatings to essentially eliminate losses, then a SPCM detection efficiency of >82% should be achievable.

### 8. Timing Resolution and Related Results

In the course of the absolute efficiency measurements a number of other effects were examined, including the effect of varying bias levels (for the SSPM), saturation (for both), temporal response (for both), and afterpulsing (for the SPCM). We will discuss these now.

The SSPM is designed to operate with a voltage bias of ~7 V. A brief investigation of the effect of different bias voltages was made at 702 nm and 633 nm; the results are plotted in Fig. 2. One should not attach too much significance to these numbers, because the amplifier bias and discriminator threshold were kept constant as the device bias was varied. It is likely that optimizing one or both of these at each device-bias level might have improved the effective efficiency. Nevertheless, for the settings used throughout most of our measurements, the device bias of 7.38 or 7.39 V seemed close to optimal, although the SSPM efficiencies in Table 1 have been adjusted upward slightly (by a 1.03 ± 0.01 correction factor) by use of the above results.

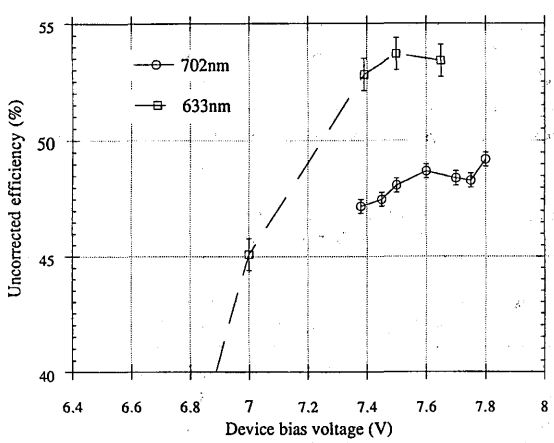


Fig. 2. Uncorrected SSPM efficiency, as a function of device-bias voltage, for fixed amplifier bias and discriminator threshold. It was not possible to check higher bias voltages because these caused the electronics to suffer frequent latch up.

By measuring the efficiency at several different pumping rates (controlled by changing the variable *ND* before the crystal), we evaluated the saturation characteristics of the detectors (see Fig. 3). The SSPM fared much better than the SPCM, which evinced a 3% efficiency reduction resulting from saturation effects for a singles rate of 100,000 $s^{-1}$. In a simplified model, the rate-dependent efficiency is given by $\eta(S_c; \delta\tau) = \eta_0(1 - S_c\delta\tau)$, where $\eta_0$ is the no-saturation limit of the measured efficiency, $S$ is the singles rate, and $\delta\tau$ is related to the detector dead time (including the subsequent electronics). Using the values from a linear fit to the saturation data, one finds $\delta\tau_{SPCM} = 0.5$ μs. (A direct measurement, described below, yielded a dead time of 1.5 μs.) A similar calculation for the SSPM yields $\delta\tau_{SSPM} = 53$ ns, which is the same as the blocking window set with the CFD.

Previous experiments have verified that the correlated photons from our source are emitted with a time correlation of better than 40 fs.[14] Thus, by looking at the coincidence time profiles in our experiment, we were able to test accurately the temporal response of the detectors at the single-photon level. Using the TAC and SCA, we took several such profiles at 702 nm with the SPCM's at various singles count rates. In particular, with the SCA in the window mode, we were able to map out the temporal profile with a 100-ps window [an example is shown in Fig. 4(a)]. Our narrowest peak was 300 ps FWHM. Because this is essentially the convolution of two SPCM's, we conclude that the time response of each is 200 ps. (Other researchers have reported even shorter time peaks with this sort of device, using custom electronics specifically designed to give a faster time response.[15]) Increasing the counting rates led to a broader profile, mainly affecting the tails. For example, the time interval necessary to catch the cen-

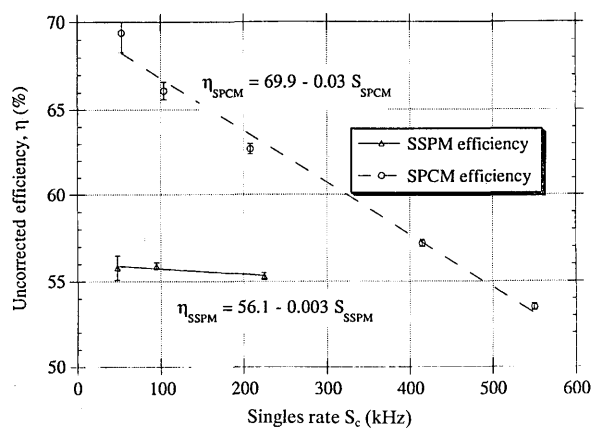


Fig. 3. Plot of uncorrected detector efficiency (at 702 nm) versus single count rate. The SSPM had a spherical mirror in place. Curves are linear fits. True efficiencies are obtained by correction for crystal losses (caused by reflection[13] and scattering or absorption), for losses at intervening optics, and for the SSPM, nonoptimal biasing.

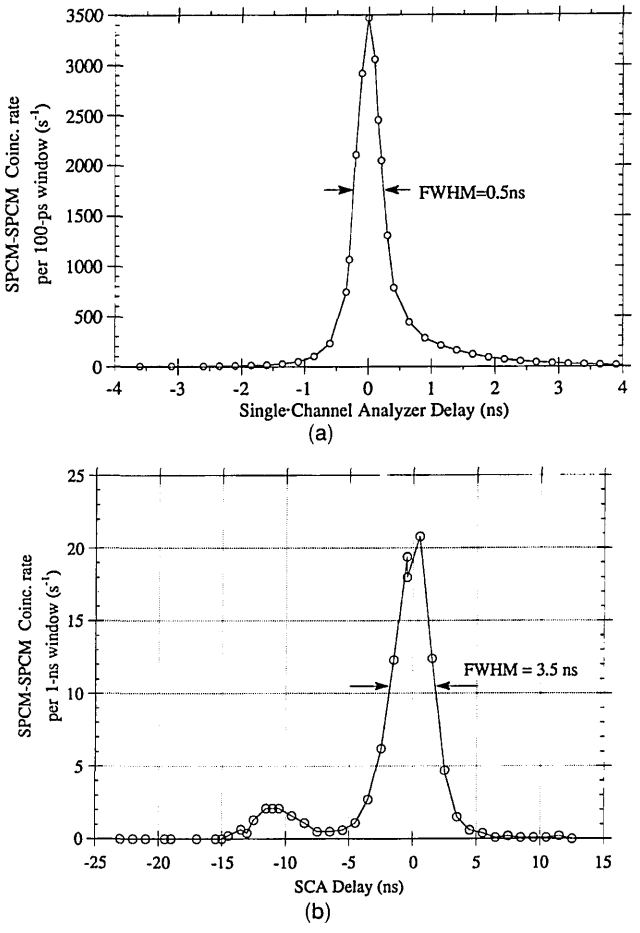


Fig. 4. Typical time-correlation profiles. (a) Coincidences between two SPCM's, with singles rates of 70 and 250 KHz. The SCA window corresponded to 100 ps; widths as low as 300 ps were seen at lower count rates. (b) Coincidences between a SSPM at a singles rate of 50 kHz and a trigger SPCM at 255 Hz. The SCA window corresponded to 1.0 ns; the spherical mirror was not in place for these measurements.

tral 80% of the coincidence counts changed from 0.5 to 1.5 ns when the detected photon rates were increased from 30,000 to 140,000 $s^{-1}$. Although it is possible that some of this saturationlike effect is due to the timing electronics (e.g., the TAC), one expects more time jitter as the count rate is increased, because of the SPCM recharging time (see below). More counts fall within the time interval during which the overbias voltage has not fully recharged; the output pulses in this case have a smaller amplitude and thus cross the preset threshold (of the leading-edge discriminator within the SPCM internal electronics) at a slightly different time.

Similar coincidence time profiles were taken (also at 702 nm) by using the SPCM trigger as the START to the TAC and a SSPM as the STOP, with a 1.0-ns SCA window [see Fig. 4(b)]. At two different pump intensity levels (SSPM, 50,000 $s^{-1}$; SSPM, 165,000 $s^{-1}$, with corresponding trigger levels of 250 and 1000 $s^{-1}$), the profiles were essentially identical. There were two peaks, a main peak (FWHM, 3.3 ns) and a smaller peak (FWHM, 4.5 ns) centered 11 ns earlier. The area under the main peak was (89.6 ± 0.5)% of the total. A second time-window measurement at 633 nm yielded consistent results for the areas under the main and precursor peaks.[16] The two peaks separated by 11 ns were not seen with two SPCM's in coincidence, and they are not expected from the model for SSPM carrier generation and transport. The initial photocarriers should appear within less than 1 ps, and their transport (ending in an avalanche) should end in less than 5 ns. The two-peak phenomenon may be caused by the associated electronic circuitry used with the SSPM.

Any single-photon detection system will have an intrinsic dead time, which will eventually limit the usable count rates, because of saturation. The SPCM's actually have two dead times associated with them. The first is a hard cutoff of 50 ns, caused by the internal shaping circuitry in the modules. The second dead time involves the time necessary to regain the high overbias voltage once an avalanche breakdown has been quenched. This is achieved in the SPCM's by charging through a ballast resistor (passive quenching). In the Geiger mode, if the bias voltage is not beyond the breakdown voltage then no avalanche can occur, and the net detector efficiency will be zero. If the bias voltage is greater than the breakdown voltage but not yet up to the standard operating point (30 V beyond avalanche breakdown, in our custom-modified detectors), then avalanche breakdown pulses will occur but the photon detection efficiency will be reduced below its maximum value. Moreover, the pulse amplitude will be less, causing increased time jitter in the leading-edge discrimination. In the course of investigating the afterpulsing characteristics of these devices (see below) we have directly measured the time constant to be 1.5 μs, which we can compare with the 0.5-μs value inferred from the saturation data. The discrepancy is due to the fact that the efficiency during the dead time is not constant, nor does it start at zero (after the 50-ns hard cutoff, during which no pulses are produced). For example, the efficiency near the beginning of the recharging dead time may be two thirds that of the maximum efficiency; then the effective dead time, to which the saturation measurements are sensitive, will be reduced from the directly observed dead time by a factor of 3.

The SSPM evinced no long-time recharging dead time because it is not operated above its avalanche breakdown voltage. We were unable to investigate intrinsic SSPM dead times less than the 50-ns CFD blocking window, which adequately accounts for the 53-ns dead time inferred from the saturation measurements. The SSPM's are expected to be continuously operating detectors for counting rates less than approximately $3 \times 10^7$ $s^{-1}$, which is the saturation rate.

It is well known that APD's operating in the Geiger mode produce afterpulses. After an avalanche, an

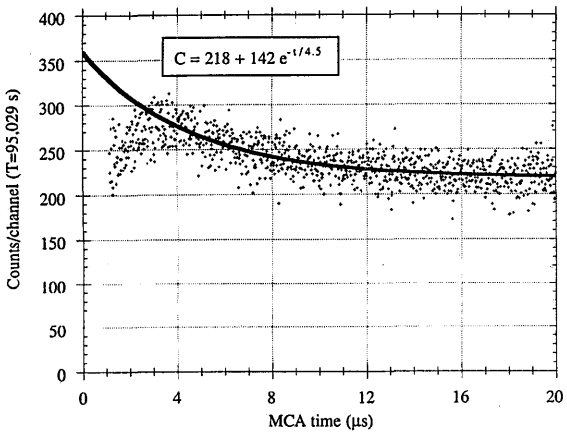


Fig. 5. Temporal autocorrelation profile of an SPCM, demonstrating afterpulsing. The solid curve is an exponential fit to the data beyond the dead-time region (~3 μs). The singles rate was 340 $s^{-1}$; total duration of measurement was 95,029 s.

impurity in the silicon may act as a trap for one of the carriers; when the trap is emptied at some random later time, a new avalanche can occur, thus causing a second pulse to be detected. We measured the presence of afterpulses by performing an autocorrelation of a SPCM with itself. The output of the detector was fed into both the START and STOP inputs of the TAC. The START pulse was delayed so that it arrived just after the STOP pulse as a way to prevent the TAC from registering a true coincidence pulse and immediately resetting. A multichannel analyzer (MCA) was used to record the profile over the ranges 2, 20, and 100 μs. Even if there were no afterpulses, one would still register counts on the MCA because of accidental coincidences. The count rate from the SPCM was therefore adjusted (by varying the input light level) to keep the accidental rate small. If the singles count rate is $S$ and if a count is registered at time $t = 0$, then the chance of registering the next count within a small interval $dt$ at time $t$ is $P(t)\ dt = S \exp^{-St}\ dt$, assuming a Poisson process. For $t \ll S^{-1}$, $P(t) \approx S(1 - St)$. For example, for the range 0–20 μs we set $S = 340\ s^{-1}$ and $t$ was always less than 20 μs, so $St < 7 \times 10^{-3}$, and we may even neglect the linear term. We counted for a total time of $T = 95{,}029$ s, and with a single-channel width of 20 μs/1024 we expect $S^2T\ dt$ to be 218 counts/channel. The presence of afterpulsing adds to this baseline a decaying structure, which is compatible with a falling exponential, with a time constant of $\tau = 4.5 \pm 0.2$ μs (see Fig. 5). If we analytically integrate the fitted exponential, we expect to find 650 ± 30 counts. A numerical summation of the data yields 400 counts, which is less because of the initial dead time. Using the larger of these results we calculate that the fraction of afterpulses is $< 2 \times 10^{-5}$, and therefore the effect on $\eta$ is negligible.

## 9. Conclusion

Our results demonstrate that suitably modified EG&G single photon counting modules can possess very high photon detection efficiencies and a relatively fast time response. It seems likely that by improvement of the AR coatings on the detector surface and the glass window of the housing, efficiencies in excess of 80% should be realizable. By increasing the overbias voltage even further, still higher efficiencies may be possible. By switching to active quenching, it should also be possible to reduce the dead time by approximately an order of magnitude. This may also help the time response at higher count rates. The primary drawback of the modules is the small active area, only ~$(100\ \mu m)^2$, which mandates careful focusing of the input light. Larger area detectors are currently under development (as are detectors using active quenching),[17] but it is unknown whether these will have as high efficiency.

The Rockwell solid-state photomultipliers had a maximum corrected efficiency of (65.6 ± 1.9)% without the spherical mirror, and (70.9 ± 1.9)% with the mirror. After the measurements and dismantling of the apparatus, the input fibers were found to have deteriorated. If these subsequently measured losses were present during the experiment and degraded the efficiency, one may conclude that the true device efficiency was as high as (93.7 ± 7.2)%. Unfortunately, there is no way to ascertain how much of this loss should be corrected for. The use of the spherical mirror definitely reduced reflection losses, increasing the efficiency by as much as 19% at 702 nm, but only by 8% at 633 nm. The presence of a 10% precursor peak in coincidence timing was surprising and is still not understood. The timing jitter we measured was probably limited by the amplifiers, so the SSPM's themselves may be somewhat faster. The main difficulty in using these detectors is the need to cool them to near-liquid-helium temperatures. Their high sensitivity in the infrared necessitates the use of some sort of cold filter (the fibers, in the system we used), which complicates input coupling. Before any further high-efficiency experiments can be performed, a better method of coupling light to the actual devices should be developed.

## Appendix A

Each experimental run to measure the efficiency coefficient consisted of two measurement periods. The first of these is the efficiency period, of duration $T$, in which the coincidences $C$ and the singles counts $S_c$ and $S_t$ (equal to the number of coincidences $C$ plus the number of anticoincidences $\alpha$) are counted. The second of these is the background period, of duration $T_{BG}$, where the source has been blocked and the trigger background counts $BG_t$ are counted. For convenience we define $r_{BG} \equiv T/T_{BG}$.

The accidental counts can be calculated from the measured quantities. There are four types of process that can yield an accidental coincidence, depending on whether the trigger count was caused by a real photon (i.e., one with a conjugate partner that could have been detected) or background, and whether the

conjugate detector count was caused by a real photon or background. In cases in which a real photon is detected, its conjugate must *fail* to be detected (otherwise this would count as a true coincidence event), so that the number of accidental counts is given by

$$A = [N_t(1 - \eta_c) + \mathrm{BG}_t r_{\mathrm{BG}}][N_c(1 - \eta_t) + \mathrm{BG}_c r_{\mathrm{BG}}]\frac{w}{T}$$

$$= (S_t - \eta_c N_t)(S_c - \eta_t N_c)\frac{w}{T}, \tag{A1a}$$

where $w$ is the duration of the gate window and we have used $S_t = N_t + \mathrm{BG}_t r_{\mathrm{BG}}$ and $S_c = N_c + \mathrm{BG}_c r_{\mathrm{BG}}$. To write Eq. (A1a) in terms of experimentally measured quantities we use the fact that $S_c \gg \eta_t N_c$ (the effective efficiency of the trigger detector is very small because of the narrow-bandwidth filter and small iris before it), and again we use $S_t = N_t + \mathrm{BG}_t r_{\mathrm{BG}}$:

$$A \approx [S_c S_t - \eta_c S_c(S_t - \mathrm{BG}_t r_{\mathrm{BG}})]\frac{w}{T}. \tag{A1b}$$

Direct measurements of the accidental rate (using an extra 100-ns electronic delay to prevent any true coincidences) were in agreement with the values obtained from approximation (A1b).

The efficiency[9] is given by the formula

$$\eta_c = \frac{C - A}{S_t - r_{\mathrm{BG}}\mathrm{BG}_t}. \tag{A2}$$

We consider the coincidences and anticoincidences during the efficiency measurement, as well as the background events, to be independent Poisson processes. In practice the uncertainty in the accidental counts was completely negligible compared with the other uncertainties. Thus we derive the statistical error on

$$\eta_c = \frac{C - A}{C + \alpha - r_{\mathrm{BG}}\mathrm{BG}_t}, \tag{A3}$$

where $\alpha = S_t - C = [(1 - \eta_c)C - A]/\eta_c + r_{\mathrm{BG}}\mathrm{BG}_t$ results from an independent Poisson process:

$$(\Delta\eta_c)^2 = \left(\frac{\partial\eta_c}{\partial C}\right)^2(\Delta C)^2 + \left(\frac{\partial\eta_c}{\partial\alpha}\right)^2(\Delta\alpha)^2 + \left(\frac{\partial\eta_c}{\partial \mathrm{BG}_t}\right)^2(\Delta \mathrm{BG}_t)^2$$

$$= \left[\frac{C + \alpha - r_{\mathrm{BG}}\mathrm{BG}_t - C + A}{(C + \alpha - r_{\mathrm{BG}}\mathrm{BG}_t)^2}\right]^2 C + \left[\frac{C - A}{(C + \alpha - r_{\mathrm{BG}}\mathrm{BG}_t)^2}\right]^2 \alpha + \left[\frac{r_{\mathrm{BG}}(C - A)}{(C + \alpha - r_{\mathrm{BG}}\mathrm{BG}_t)^2}\right]^2 \mathrm{BG}_t. \tag{A4}$$

$$\left(\frac{\Delta\eta_c}{\eta_c}\right)^2 = \frac{1}{(C - A)^2}[(1 - \eta_c)^2 C + \eta_c{}^2\alpha + r_{\mathrm{BG}}{}^2\eta_c{}^2\mathrm{BG}_t]$$

$$= \frac{1}{(C - A)^2}[(1 - \eta_c)C + r_{\mathrm{BG}}(1 + r_{\mathrm{BG}})\eta_c{}^2\mathrm{BG}_t]. \tag{A5}$$

$$\frac{\Delta\eta_c}{\eta_c} = \left\{\frac{1}{(C - A)^2}[(1 - \eta_c)C + r_{\mathrm{BG}}(1 + r_{\mathrm{BG}})\eta_c{}^2\mathrm{BG}_t]\right\}^{1/2}. \tag{A6}$$

In practice the time intervals over which the trigger singles and background counts were collected were similar ($r_{\mathrm{BG}} \approx 1$), so Eq. (A6) simplifies to

$$\frac{\Delta\eta_c}{\eta_c} = \left[\frac{(1 - \eta_c)C}{(C - A)^2} + \frac{2\mathrm{BG}_t}{(S_t - \mathrm{BG}_t)^2}\right]^{1/2}. \tag{A7}$$

The SSPM's were developed at Rockwell Science Center, Anaheim; the specific devices used in the measurements reported here were prepared for the University of California, Los Angeles as part of a program sponsored by the U.S. Department of Energy, directed by M. Atac (of Fermilab and the University of California, Los Angeles). We thank M. Atac for generously allowing the use of the SSPM's. We also gratefully acknowledge the assistance and input of B. Johnson and R. Ross and helpful discussions with R. J. McIntyre. Three of us (P. G. K., A. M. S., and R. Y. C.) are supported by the U.S. Office of Naval Research under grant N00014-90-J-1259. One of us (P. H. E.) is supported by the U.S. Department of Energy, contract DE-AC03-76SF00098.

## References and Notes

1. M. D. Petroff, M. G. Stapelbroek, and W. A. Kleinhans, "Detection of individual 0.4–28 μm wavelength photons via impurity-impact ionization in a solid-state photomultiplier," Appl. Phys. Lett. **51,** 406–408 (1987).
2. A. W. Lightstone, A. D. MacGregor, D. E. MacSween, R. J. McIntyre, C. Trottier, and P. P. Webb, "Photon counting modules using RCA silicon avalanche photodiodes," Electron. Eng. **61,** 37–47 (1989).
3. P. G. Kwiat, A. M. Steinberg, R. Y. Chiao, P. H. Eberhard, and M. D. Petroff, "High efficiency single-photon detectors," Phys. Rev. A **48,** R867 (1993).
4. J. G. Rarity, P. R. Tapster, J. A. Levenson, J. C. Garreau, I. Abram, J. Mertz, T. Debuisschert, A. Heidmann, C. Fabre, and E. Giacobino, "Quantum correlated twin beams," Appl. Phys. B **55,** 250–257 (1992).
5. A. Yariv, *Quantum Electronics,* 3rd ed. (Wiley, New York, 1988), Chap. 7, p. 430.
6. C. K. Hong and L. Mandel, "Theory of parametric frequency down conversion of light," Phys. Rev. A **31,** 2409–2418 (1985).
7. D. N. Klyshko, "Use of two-photon light for absolute calibration of photoelectric detectors," Sov. J. Quantum Electron. **10,** 1112–1116 (1980).
8. J. G. Rarity, K. D. Ridley, and P. R. Tapster, "Absolute measurement of detector quantum efficiency using parametric downconversion," Appl. Opt. **26,** 4616–4619 (1987).
9. Because of saturation effects (arising from intrinsic dead time

in the devices), the efficiency actually depends on the incident light intensity (see Section 8 in the text). However, for simplicity we use $\eta$ to denote the efficiency in the low-light limit.
10. H. Z. Cummins and E. R. Pike, eds., *Photon Correlation and Light Beating Spectroscopy* (Plenum, New York, 1974).
11. R. J. McIntyre, "On the avalanche initiation probability of avalanche diodes above the breakdown voltage," IEEE Trans. Electron. Devices **20,** 637–641 (1973).
12. R. J. McIntyre, Optoelectronics Division, EG&G Canada, Ltd., 22001, Dumberry, Vaudreuil J7V 8P7, Canada (personal communication, 1993).
13. A secondary measurement revealed that the reflection intensity off the crystal input face (coated for low loss at 351 nm) was (3.37 ± 0.38)%. In a few of the runs the crystal was accidentally inserted backward; in these cases, the reflection losses are those from the 351-nm coating. This correction is included in Table 1, where appropriate.
14. A. M. Steinberg, P. G. Kwiat, and R. Y. Chiao, "Dispersion cancellation in a measurement of the single-photon propagation velocity in glass," Phys. Rev. Lett. **68,** 2421–2424 (1992).
15. L. Q. Li, L. M. Davis, S. I. Soltesz, and C. J. Trottier, "Single-photon avalanche diode for single molecule detection," in *OSA Annual Meeting,* Vol. 23 of OSA 1992 Technical Digest Series (Optical Society of America, Washington, D.C., 1992).
16. At one point a fast oscilloscope (triggered on the trigger-detector output) was used to observe the coincidence pulses. No precursors were observed, but two of the ten coincident pulses were delayed by ~20 ns relative to the other eight. The probability of these being accidental is very small. However, these postcursors were not seen on a second scope trace with 14 coincidence events displayed.
17. A. D. MacGregor, Optoelectronics Division, EG&G Canada, Ltd., 22001 Dumberry, Vaudreuil J7V 8P7, Canada (personal communication, 1992).